ACS APPLIED MATERIALS & INTERFACES

Research Article

www.acsami.org

Morphology Change and Improved Efficiency in Organic Photovoltaics via Hexa-*peri*-hexabenzocoronene Templates

Henk H. Dam,[†] Kuan Sun,[†] Eric Hanssen,[‡] Jonathan M. White,[†] Tomasz Marszalek,[§] Wojciech Pisula,[§] Jens Czolk,[∥] Jens Ludwig,[∥] Alexander Colsmann,[∥] Marina Pfaff,[⊥] Dagmar Gerthsen,[⊥] Wallace W. H. Wong,*[,†] and David J. Jones*[,†]

[†]School of Chemistry, Bio21 Institute, The University of Melbourne, 30 Flemmington Road, Parkville, Victoria 3010, Australia

[‡]Advanced Microscopy Facility, Bio21 Institute, The University of Melbourne, 30 Flemington Road, Parkville, Victoria 3010, Australia

[§]Max-Planck-Institute for Polymer Research, Ackermannweg 10, Mainz 55128, Germany

[∥]Lichttechnisches Institut, Karlsruhe Institute of Technology, Engesserstrasse 13, Karlsruhe 76131, Germany

[⊥]Laboratorium für Elektronenmikroskopie, Karlsruhe Institute of Technology, Engesserstraße 7, Karlsruhe 76131, Germany

Supporting Information

ABSTRACT: The morphology of the active layer in organic photovoltaics (OPVs) is of crucial importance as it greatly influences charge generation and transport. A templating interlayer between the electrode and the active layer can change active layer morphology and influence the domain orientation. A series of amphiphilic interface modifiers (IMs) combining a hydrophilic polyethylene-glycol (PEG) oligomer and a hydrophobic hexabenzocoronene (HBC) were designed to be soluble in PEDOT:PSS solutions, and surface accumulate on drying. These IMs are able to self-assemble in solution. When IMs are deposited on top of a poly(3,4-ethylenedioxythiophene) poly(styrenesulfonate) (PEDOT:PSS) film, they induce a morphology change of the active layer consisting of discotic fluorenyl-substituted HBC (FHBC) and [6,6]-phenyl C_{61}-butyric acid methyl ester (PCBM). However, when only small amounts (0.2 wt %) of IMs are blended into PEDOT:PSS, a profound change of the active layer morphology is also observed. Morphology changes were monitored by grazing incidence wide-angle X-ray scattering (GIWAXS), transmission electron microscopy (TEM), TEM tomography, and low-energy high-angle angular dark-field scanning transmission electron microscopy (HAADF STEM). The interface modification resulted in a 20% enhancement of power conversion efficiency.

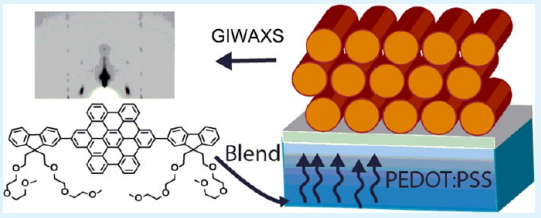

KEYWORDS: *organic solar cell, morphology control, template, surface modification, molecule diffusion*

INTRODUCTION

Device performance of bulk heterojunction (BHJ) organic photovoltaics (OPVs) is strongly linked to charge carrier generation and transport, which are closely related to the morphology of the active layer. The exciton diffusion limit in organic semiconductors of 5−15 nm sets an upper limit for the donor domain sizes.[1,2] The donor and acceptor blend must form a bicontinuous interpenetrating network to allow efficient charge transport to the electrodes. Charge transport can be improved by ordered or crystalline domains that provide high charge carrier mobilities. The active layer morphology can be influenced by common methods including thermal annealing,[3,4] solvent annealing,[5,6] use of cosolvents,[7−10] solvent additives,[11−13] or solid additives.[14] These methods, however, lack in the ability to induce a preferential orientation of molecules in the domains that can be beneficial for the efficient extraction of charge carriers from the bulk heterojunction. For example, self-assembly by $\pi-\pi$ stacking can lead to a columnar mesophase of polycyclic aromatic hydrocarbons (PAHs), which exhibit anisotropic semiconducting properties with charge and exciton mobilities being the highest along the main axis of the columns.[15−20]

Hexa-*peri*-hexabenzocoronenes (HBCs) are an illustrative example of PAHs that have a high tendency to self-assemble into columnar structures[21−23] and display a high charge carrier mobility along their main columnar axis.[14,20] In organic field effect transistor (OFET) devices, a hole mobility of 2.8×10^{-3} $cm^2 \cdot V^{-1} \cdot s^{-1}$ was observed for fluorenyl-substituted HBC, whose chemical structure is shown in Chart 1.[24] Substrate−HBC interactions are the main driving force for controlled directional growth of HBC molecules.[20,25−28] The directional growth of HBC columns can also be controlled by using a monolayer of HBCs as a nucleation site.[20,25]

Our goal is to advantageously change the morphology, that is, the domain sizes, crystal packings, or the orientation of molecules of an active layer via a templating strategy. This can be accomplished by inserting a templating interlayer at the

Received: March 18, 2014
Accepted: May 9, 2014
Published: May 21, 2014

   dx.doi.org/10.1021/am5015666 | ACS Appl. Mater. Interfaces 2014, 6, 8824−8835

Chart 1. Chemical Structures of the Donor (FHBC) and Acceptor (PCBM) Used in This Study

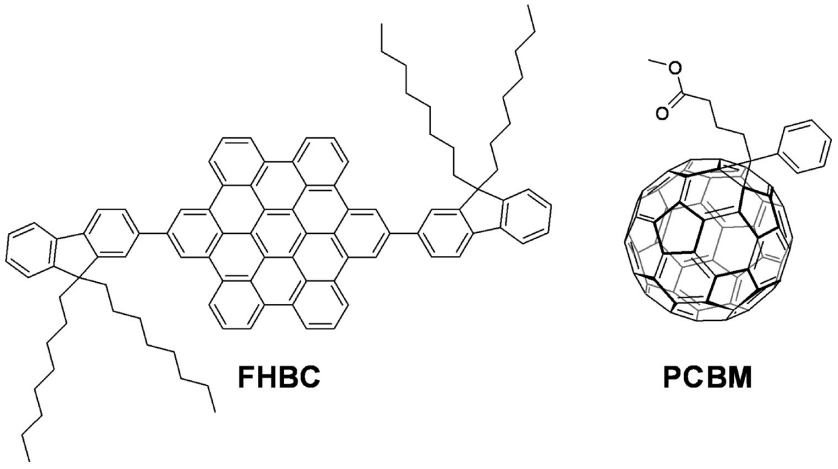

Chart 2. Chemical Structures of the Interface Modifiers (IMs) Used in This Study[a]

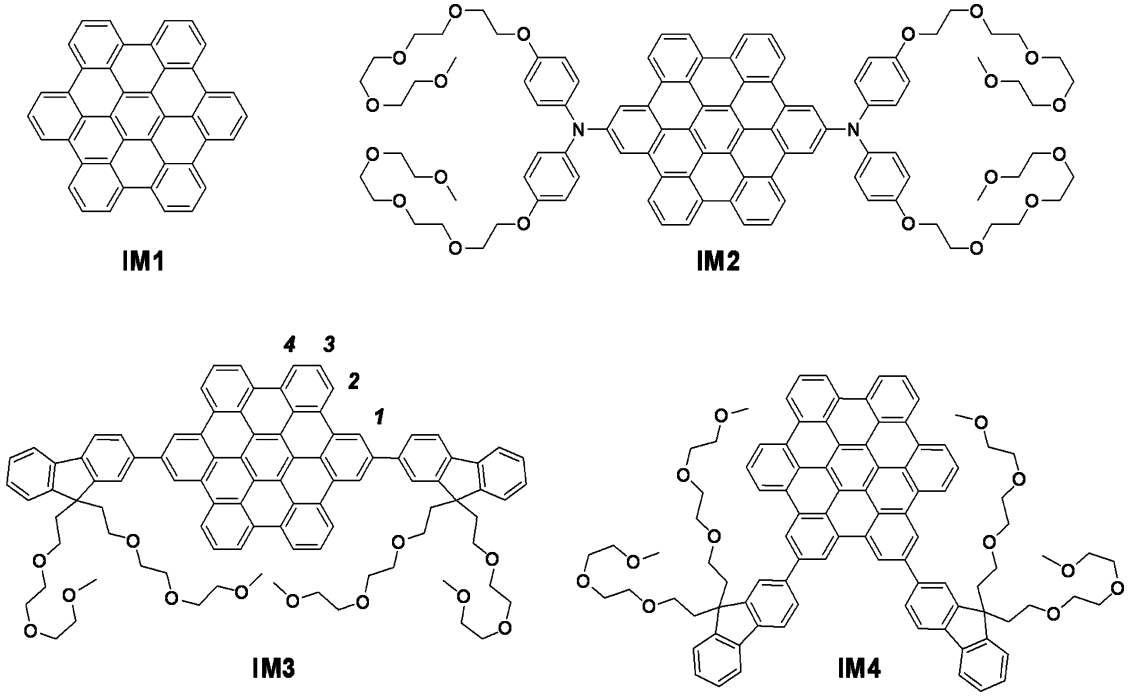

[a]Protons identified in solution aggregation NMR studies are numbered **1**–**4** on **IM3**.

electrode/active layer interface. However, to increase processability and reduce the number of processing steps for roll-to-roll production of OPVs, we aimed to develop a strategy that avoids the additional deposition step of the interlayer compound. This strategy, described herein, is based on the blending of amphiphilic organic compounds into the poly(3,4-ethylenedioxythiophene):poly(styrenesulfonate) (PEDOT:PSS) layer aiming to exploit the potential surface diffusion and self-assembly of such molecules because of hydrophilic–hydrophobic interactions and the subsequent formation of an interlayer. In addition, by judicious selection of the appropriate amphiphilic unit, such as an ethylene glycol oligomer, the conductivity of the PEDOT:PSS layer may be improved thereby improving device performance. We demonstrate that blending of only a small amount of amphiphilic discotic interface modifier (abbreviated as IM, chemical structures shown in Chart 2) into a PEDOT:PSS solution prior to its deposition can have a profound effect on the morphology of the layer deposited on top of this substrate mixture and the efficiency of an OPV device.

Amphiphilic IMs based on the HBC core with small PEG moieties were synthesized and fully characterized. Their surface accumulation characteristics and effect on the morphology of an active layer containing either 2,11-bis(9,9-dioctyl-9*H*-fluoren-2-yl)hexabenzo-[bc,ef,hi,kl,no,qr]coronene[24] (FHBC) only or a blend with [6,6]-phenyl C_{61}-butyric acid methyl ester (PCBM) (Chart 1) were studied. Furthermore, their effect on the performance of OPV devices consisting of a FHBC:PCBM active layer was studied.

EXPERIMENTAL METHODS

Film Characterization. Atomic force microscopic (AFM) images were acquired with an Asylum Research Cypher scanning probe microscope operated in tapping mode. Contact angle measurements

were performed using the sessile drop method on a goniometer (Ramé-Hart Inc.). The contact angle of each substrate was measured at four locations and their average values are shown. The work function of the substrates was estimated by photoelectron spectroscopy in air (PESA), which was conducted on a Riken Keiki AC-2 spectrometer. A power intensity of 5 nW was used during the measurement. The sheet resistance was measured with a Jandel cylindrical four point probe at room temperature.

Bright-field and dark-field transmission electron microscopy (TEM) images and selected area electron diffraction (SAED) patterns were obtained with a FEI Tecnai TF30 transmission electron microscope operated at 300 keV and equipped with beam blank function. High-angle annular dark-field scanning transmission electron microscopy (HAADF STEM) was performed at a primary electron energy of 15 keV with a FEI Quanta 3D microscope equipped with a HAADF STEM detector. Electron transparent samples for TEM were prepared by the following procedure. First, a scalpel was used to cut the organic film dividing it into small segments (~2 × 2 mm). As poly(3,4-ethylenedioxythiophene):poly(styrenesulfonate) (PEDOT:PSS) is water-soluble, the pieces of the active layer can be floated off the substrate by a drop of water from where they can be transferred onto conventional TEM copper grids. For electron tomography, the same TEM samples loaded with gold fiducial markers of 10 nm in diameter were used. Tilt series were acquired using the Xplore 3D software (FEI Company). Tomograms were recorded between −65 and +65 degrees at 2° intervals and aligned with IMOD.[29] The 3D model rendering was achieved using 3dmod software.[30] Each model was generated from the aligned tomogram. The FHBC donor phase was rendered in golden color, while the PCBM acceptor phase was represented by empty space in the Supporting Information movie. The scale bar was 50 nm in this model movie.

Grazing incidence wide-angle X-ray scattering (GIWAXS) was recorded at the small/wide-angle X-ray scattering beamline at the Australian Synchrotron. The samples were prepared on PEDOT:PSS coated glass substrates. Eleven kiloelectron volt photon energy and a PILATUS 1 M detector were used in the setup. The sample-to-detector distance was calibrated using a silver behenate standard. Data acquisition time is 3 s to minimize any alteration or damage of the sample. Each image was photostitched from three continuous images.

Interface Modification. Three different methods were employed for the fabrication of films with an interlayer, as illustrated in Chart 3.

Chart 3. Schematic Drawing of the Deposition Processes of IMs[a]

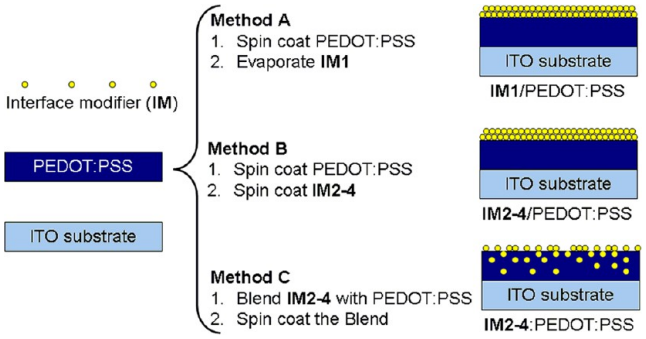

[a]The diagrams are not drawn to scale.

IM2/PEDOT:PSS, **IM3**/PEDOT:PSS, and **IM4**/PEDOT:PSS films (note the slash used in the name) were prepared by spin-coating the IMs (1 mg/mL in 1,4-dioxane, 1500 rpm, 40 s) onto PEDOT:PSS coated glass, followed by annealing in air at 150 °C for 10 min. **IM2**:PEDOT:PSS, **IM3**:PEDOT:PSS, and **IM4**:PEDOT:PSS (note that here a colon is used in the name) films were prepared by mixing the IMs (30 μL, 1 mg/mL in 1,4-dioxane) with 1 mL of PEDOT:PSS (Heraeus Clevios VP AI 4083) aqueous solution (0.2 wt % IM in PEDOT:PSS). The resulting mixture was spin-coated (5000 rpm, 40 s) onto glass followed by annealing in air at 150 °C for 10 min. Because of limited solubility of the unsubstituted HBC **IM1** in PEDOT:PSS aqueous solution, **IM1**/PEDOT:PSS films were prepared by thermally evaporating HBC molecules under vacuum onto a PEDOT:PSS layer. This method allows a precise control over the thickness of the resulting HBC layer.[31]

Device Fabrication and Characterization. All the fabrication and characterization processes were carried out in air. Patterned indium tin oxide (ITO) glasses were washed in the following order by detergent, deionized water, acetone, and 2-propanol using ultrasonication and, subsequently, UV/ozone-treated. PEDOT:PSS was spin-coated on top (8000 rpm) and the resulting layer was annealed (150 °C for 10 min) in air. After it was cooled to room temperature, a solution consisting of recrystallized FHBC (8 mg) and PCBM (16 mg) in chlorobenzene (1 mL) was spin-coated on top (1000 rpm) in air. The films were transferred to a thermal evaporator where 1 nm LiF and 100 nm aluminum were deposited through a shadow mask (active area of 0.10 cm^2) at a base pressure of 1×10^{-6} Torr. No thermal annealing was carried out. Film thicknesses were determined with a Veeco Dektak 150+ Surface Profiler. The thicknesses of the photoactive layers were optimized to 60−70 nm. The solar cells were illuminated at 100 mW cm^{-2} using 1 kW Oriel solar simulator with an AM 1.5G filter in air and $J-V$ curves were measured using a Keithley 2400 source meter. For accurate measurement, the light intensity was calibrated using a reference silicon solar cell (PVmeasurements Inc.) certified by the National Renewable Energy Laboratory. Series resistance (R_s) and shunt resistance (R_{sh}) were derived from dark currents by taking the reciprocal of the slopes at 1.5 and 0 V, respectively.

RESULTS AND DISCUSSION

Synthesis of Interface Modifiers (IMs). The interface modifier **IM1** was synthesized from hexaphenylbenzene via oxidative dehydrogenation according to literature methods.[4] The synthesis of the amphiphilic HBC **IM2** was achieved via Pd(0) catalyzed Buchwald-Hartwig coupling of ethylene glycol substituted phenylamine **5** and dibromo-functionalized HBC **6** in 73% yield (Supporting Information Scheme S1). The ethylene glycol substituted phenylamine **5** had to be dried at 60 °C under vacuum for 3 h for the Buchwald coupling to proceed smoothly (see Supporting Information for details on the synthesis). Additionally, the low solubility of dibromo-functionalized HBC **6** meant that it was essential to disperse compound 6 using ultrasonication for the reaction. The interface modifiers **IM3** and **IM4** were obtained via a Suzuki coupling between 9,9-bis(triethylene glycol monomethyl ether)-substituted fluorenyl unit (**9**) and *para*- or *ortho*-dibromo-HBC cores (**6** or **10**) (Supporting Information Scheme S2). The compounds **IM3** and **IM4**, which can be purified by column chromatography with SiO_2, were synthesized in a yield of 19% and 16%, respectively. The yield of **IM4** can be improved to 34% by purification with size exclusion chromatography (see Supporting Information for details).

Self-Association of IM3 in $CDCl_3$. The self-association properties of the amphiphilic compounds were initially assessed in solution by examining the NMR spectra of the compounds at various concentrations. Analogues of **IM3** and **IM4** having octyl moieties instead of PEG have been studied before in this manner in our group.[24] In these studies, upfield shift of the resonances belonging to the hydrogen atoms on the HBC core was observed with increasing concentration of the compounds in the ^{1}H NMR spectrum. This is indicative of staggered $\pi-\pi$ stacking of the HBC molecules where the HBC aromatic hydrogen atoms are deshielded by the proximity of adjacent HBC molecules.[24] In a similar manner, we observed shifts in the HBC-ring protons in the ^{1}H NMR spectra of **IM2**−**IM4**

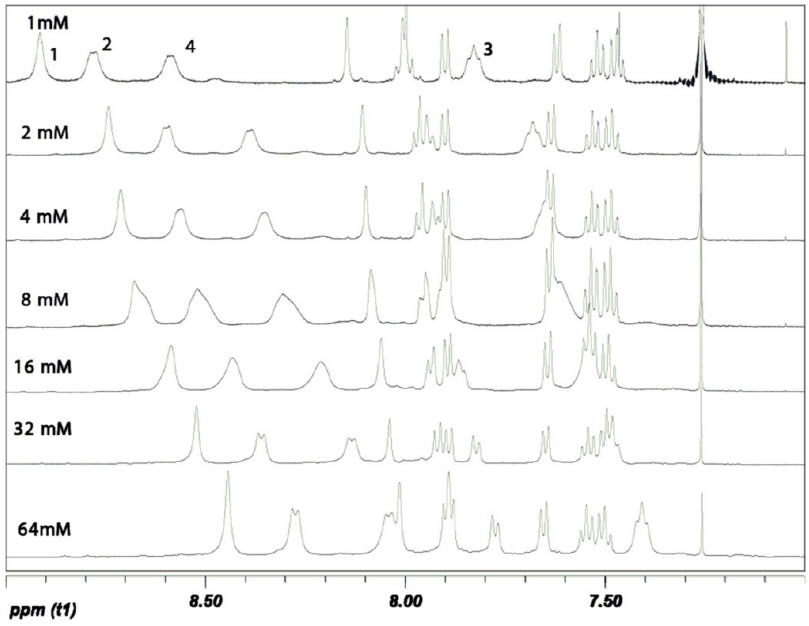

Figure 1. Concentration-dependent ^{1}H NMR spectra of compound **IM3** (20 °C). Assignments of the peaks were performed by comparison with spectra of known materials.[24] The bold numbers refer to the hydrogens of **IM3** as shown in Chart 2

when changing their concentrations in $CDCl_3$. A more detailed examination of this effect was performed on **IM3** by taking its ^{1}H NMR spectra in a concentration range from 1 mM to 64 mM (Figure 1). The change in chemical shift observed for the HBC-core protons **1**−**4** from 1 to 64 mM solution is about 0.5 ppm which is similar to that of the FHBC compound examined in previous studies.[24] The NMR data suggest that the PEG moieties are not interfering with the self-assembly of compound **IM3** into columnar structures.

Characterization of Modified Interfaces. A layer of interface modifier onto PEDOT:PSS was obtained via three different methods (Chart 3). Method A utilized vacuum technology to thermally evaporate **IM1** on top of PEDOT:PSS, because **IM1** has a very limited solubility in most solvents.[31] Using this method, the thickness of the **IM1** layer can be controlled precisely. The sample is denoted as "**IM1**/PEDOT:PSS". In method B, 1 mg/mL 1,4-dioxane solutions of **IM2**−**4** were spin-coated at a spin rate of 1500 rpm onto PEDOT:PSS coated glass, followed by annealing in air at 150 °C for 10 min. The interlayer is denoted as "**IM2**−**4**/PEDOT:PSS". In Method **C**, 30 μL of 1 mg/mL 1,4-dioxane solutions of **IM2**−**4** were added into 1 mL of PEDOT:PSS aqueous solution to make a weight ratio of 0.2% between **IM2**−**4** and PEDOT:PSS solid content. The blended solution was then used to form the interlayer by spin-coating at 5000 rpm followed by thermal annealing. The interlayer fabricated in this way is denoted as "**IM2**−**4**:PEDOT:PSS".

The surface morphologies of the PEDOT:PSS, **IM**/PEDOT:PSS, and **IM**:PEDOT:PSS films were studied by AFM. Presumably because of the small amount of IMs introduced, a significant visual change in surface topography could not be observed. A more quantitative analysis can be obtained from the root-mean-square roughness (R_{rms}). The evaporation of **IM1** on top of PEDOT:PSS (Figure 2b) results in an increase in R_{rms}, from 0.71 to 0.85 nm. It is likely that the HBC molecules assemble edge-on in order to minimize contact with the hydrophilic PEDOT:PSS substrate and to maximize intermolecular π−π−stacking interactions. Spin-coating a layer of IM2 on top of PEDOT:PSS (Figure 2c) gave a larger R_{rms} probably as a result of aggregation of **IM2** molecules. On the other hand, the deposition of **IM3** and **IM4** on top of PEDOT:PSS (Figure 2i, k) resulted in smoother surfaces with 20−40% decrease in R_{rms}. The IM:PEDOT:PSS blend films (Figure 2d, j, l), generally increase the R_{rms}, implying the presence of IMs on PEDOT:PSS surface.

Compared to a pure PEDOT:PSS film (Figure 2e), the evaporation of an **IM1** layer on top of PEDOT:PSS to give **IM1**/PEDOT:PSS (Figure 2f) resulted in the most pronounced reduction in phase contrast. Most likely, the phase contrast originating from the difference in material stiffness between PEDOT and PSS is largely reduced because of effective screening by the **IM1** layer.[32] Despite that, pin holes are still observed as black spots suggesting an incomplete coverage of the surface by **IM1**. The phase contrast of the **IM2**−**4**/PEDOT:PSS and **IM2**−**4**:PEDOT:PSS films are also slightly reduced which suggests the presence of amphiphilic IM on the surface.

Further evidence of the presence of IMs on PEDOT:PSS surface was obtained from contact angle and photoelectron spectroscopy in air (PESA) measurements. Table 1 shows there is a slight increase in the contact angles of water on the IM/PEDOT:PSS and IM:PEDOT:PSS films as compared to the PEDOT:PSS substrate. Since PEDOT:PSS is hydrophilic while **IM1** and the core of **IM2**−**4** are hydrophobic, the increase in the contact angles suggests that there are IMs present at the surface of the IM:PEDOT:PSS and IM/PEDOT:PSS films.

The ionization potential (IP), obtained with PESA, of the PEDOT:PSS film dropped by more than 0.3 eV after coating with IMs (Table 1). The IP decreases slightly when the PEDOT:PSS is blended with **IM3** or **IM4**. The lowest IP was observed for **IM2**/PEDOT:PSS, which is consistent with the lower HOMO level of **IM2** (−4.8 eV) as compared to **IM3** (−4.9 eV) and **IM4** (−5.1 eV), as determined by cyclic voltammetry (Supporting Information Figure S1).

Interestingly, the modification of the PEDOT:PSS layer by IMs resulted in a small reduction of the sheet resistance of the

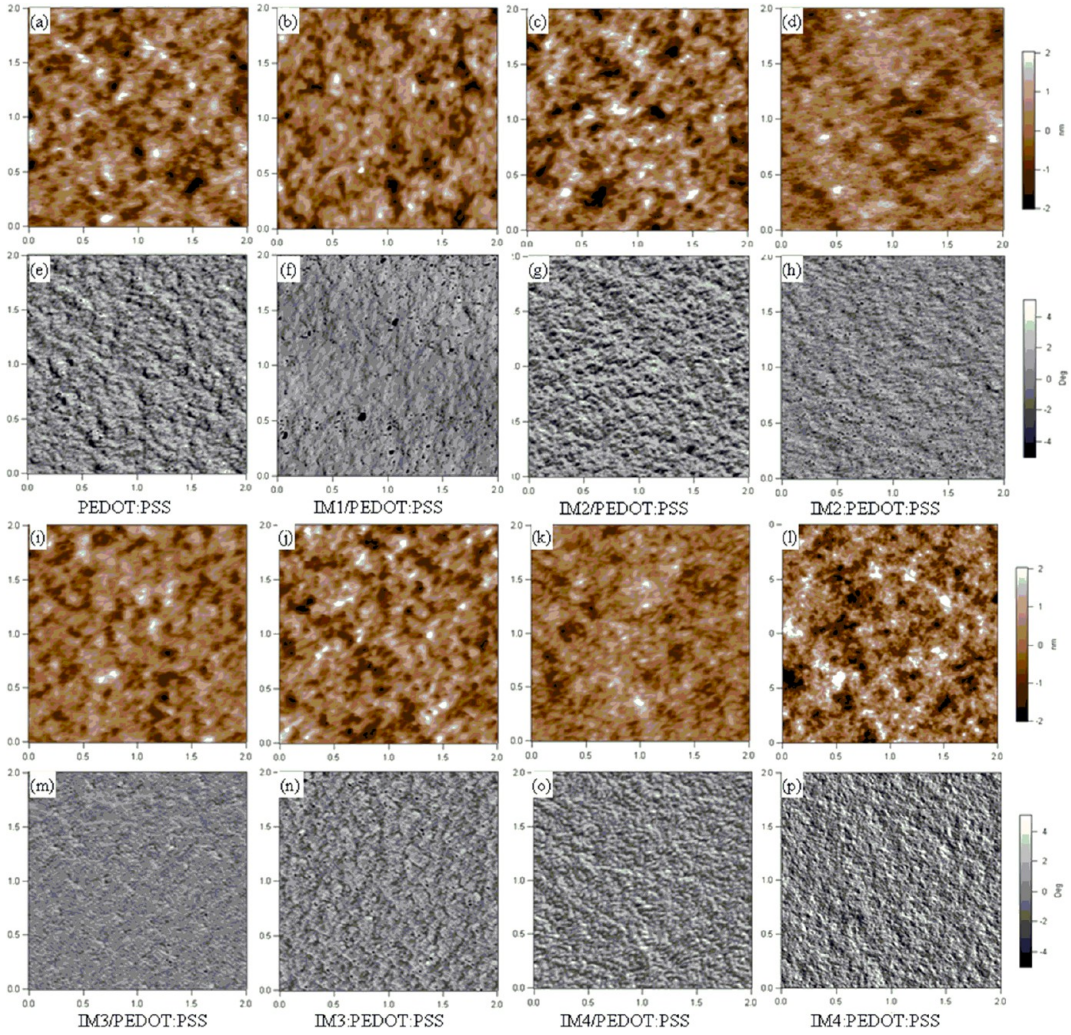

Figure 2. AFM height images (a–d and i–l) and phase images (e–h and m–p) of PEDOT:PSS, IM/PEDOT:PSS, and IM:PEDOT:PSS films. The root-mean-square roughness (nm) of these samples are 0.71 (a), 0.85 (b), 0.79 (c), 0.87 (d), 0.57 (i), 0.70 (j), 0.53 (k), and 0.84 (l). The image size is 2 μm × 2 μm. The height bar scale is 4 nm and the phase contrast scale is 10 degrees.

Table 1. Contact Angles, Ionization Potentials (IP), and Sheet Resistances of Substrate PEDOT:PSS, IM/PEDOT:PSS, and IM:PEDOT:PSS Films

film	contact angle (deg)	IP (eV)	sheet resistance (MΩ/Sq.)
PEDOT:PSS	8.7 ± 0.7	5.32	820
IM1/PEDOT:PSS	18.4 ± 1.5	5.05	362
IM2/PEDOT:PSS	14.5 ± 1.7	4.85	44
IM3/PEDOT:PSS	15.3 ± 2.1	5.06	127
IM4/PEDOT:PSS	12.1 ± 1.9	5.02	331
IM2:PEDOT:PSS	12.9 ± 1.7	5.32	122
IM3:PEDOT:PSS	13.8 ± 1.3	5.22	54
IM4:PEDOT:PSS	12.5 ± 2.0	5.24	45

PEDOT:PSS films (Table 1). Previous studies showed enhancement of PEDOT:PSS film conductivity after treatment by ethylene glycol and poly(ethylene glycol) (PEG), both can form hydrogen bonds with protonated PSS, resulting in weakening of the columbic interaction between PEDOT and PSS. 'This can lead to a more enhanced/pronounced PEDOT chain conformation and an increase of its interchain interaction, resulting in an enhanced conductivity.[33,34] The PEG chains of **IM2–4** in our case might have a similar effect. In other words, it implies the PEG groups can interact strongly with PEDOT:PSS and act as anchoring groups.

Photovoltaic Performance. The effect of interface modification by IMs on the morphology of the subsequently deposited FHBC:PCBM (1:2 weight ratio) bulk heterojunction was examined in terms of photovoltaic performance. All solar cell fabrication and characterization were performed in air. No thermal annealing of the active layer was carried out. Deposition of all four IMs on top of PEDOT:PSS improves the fill factor (FF), from 56% to over 60% (Figure 3 and Table 2). The presence of a spin-coated **IM3** results in a 20% improvement of power conversion efficiency (PCE) to 1.6%, which is due to increased short-circuit current density (J_{sc}) (2.66 mA/cm^2) and FF (65%). For all OPVs with **IM2–4**/PEDOT:PSS interlayers, a reduction in V_{oc} is observed. Zhou et al. reported that PEG can form a surface dipole in such a way that the work function is lowered.[35] In a similar manner the reduced work function observed for the IM/PEDOT:PSS films might originate from a surface dipole effect due to the PEG moieties of **IM2–4**. The lowering of the work function results in an energy level mismatch at the anode/active layer interface with a concomitant reduction in the V_{oc} of the OPV devices.

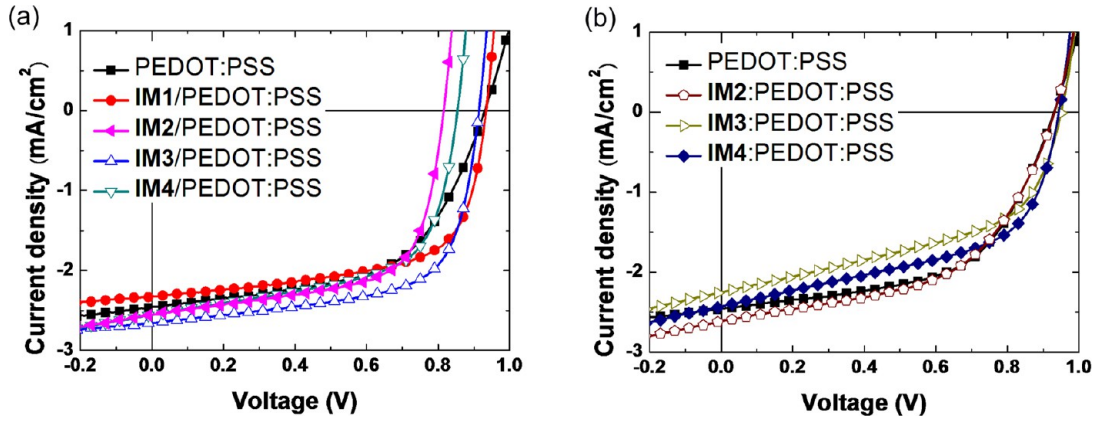

Figure 3. $J-V$ curves of OPVs based on FHBC:PCBM (1:2) with different anode interlayers (a) **IM**/PEDOT:PSS and (b) **IM**:PEDOT:PSS tested under 1 sun condition (100 mW/cm^2).

Table 2. Photovoltaic Performance Parameters of OPVs Based on FHBC:PCBM with Different IM Layers Tested under 1 Sun Illumination (100 mW/cm^2)[a]

anode interlayers	V_{oc} (V)	J_{sc} (mA/cm^2)	FF (%)	PCE (%)	R_s (Ω/cm^2)	R_{sh} (Ω/cm^2)
PEDOT:PSS	0.92 ± 0.01 (0.93)	2.0 ± 0.4 (2.5)	54 ± 3 (56)	1.0 ± 0.2 (1.3)	4.1	16 703
IM1/PEDOT:PSS	0.94 ± 0.01 (0.93)	2.0 ± 0.20 (2.3)	63 ± 2 (64)	1.2 ± 0.1 (1.4)	2.6	37 383
IM2/PEDOT:PSS	0.81 ± 0.02 (0.82)	2.4 ± 0.3 (2.6)	63 ± 3 (64)	1.2 ± 0.1 (1.3)	3.1	92 764
IM3/PEDOT:PSS	0.91 ± 0.01 (0.91)	2.4 ± 0.2 (2.7)	64 ± 3 (65)	1.4 ± 0.2 (1.6)	5.1	36 846
IM4/PEDOT:PSS	0.82 ± 0.01 (0.85)	2.5 ± 0.1 (2.6)	60 ± 5 (61)	1.2 ± 0.1 (1.3)	2.4	106 952
IM2:PEDOT:PSS	0.90 ± 0.02 (0.93)	2.1 ± 0.4 (2.6)	48 ± 3 (53)	0.9 ± 0.3 (1.3)	2.4	4855
IM3:PEDOT:PSS	0.94 ± 0.01 (0.95)	1.9 ± 0.3 (2.3)	49 ± 1 (50)	0.9 ± 0.2 (1.1)	5.4	1563
IM4:PEDOT:PSS	0.93 ± 0.01 (0.94)	2.1 ± 0.2 (2.4)	51 ± 2 (54)	1.0 ± 0.1 (1.2)	2.8	5878

[a]Average device parameter values and the standard deviation for six devices are shown with the values for the best device in brackets.

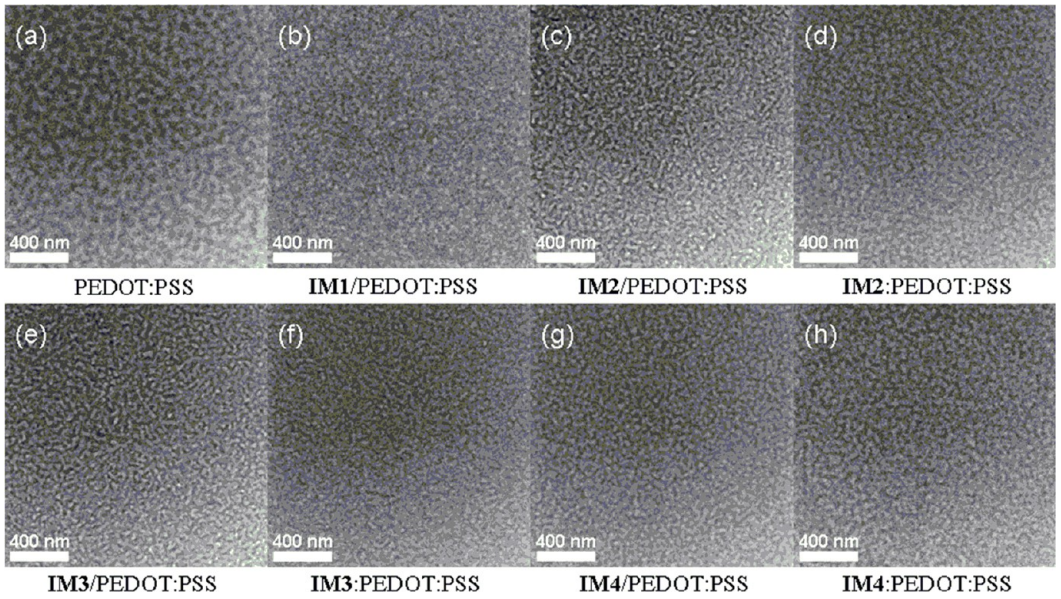

Figure 4. 300 keV Bright-field TEM images of FHBC:PCBM (1:2) blend films on various substrates (a) PEDOT:PSS; (b, c, e, g) **IM**/PEDOT:PSS and (d, f, h) **IM**:PEDOT:PSS. All films have the same magnification, the scale bar is 400 nm.

This hypothesis is supported by the observation that **IM1**, which lacks the PEG moieties, does not change the V_{oc}.

Blending IMs into PEDOT:PSS does not improve the overall device performance. The devices suffer from low FFs. The dark $J-V$ curves (Supporting Information Figure S2) suggest that the reduced FF originates mainly from a smaller shunt resistance, which is reduced by at least 1 order of magnitude (Table 2). Possibly the **IM**:PEDOT:PSS interlayers with reduced sheet resistance provides a pathway for leakage current.

Thin Film Characterization of FHBC:PCBM Blend Films. To obtain a better understanding of the origin of the effect IMs have on the photovoltaic parameters, we studied the morphology of the FHBC:PCBM (1:2) active layers using TEM, HAADF STEM and TEM tomography. FHBC is less

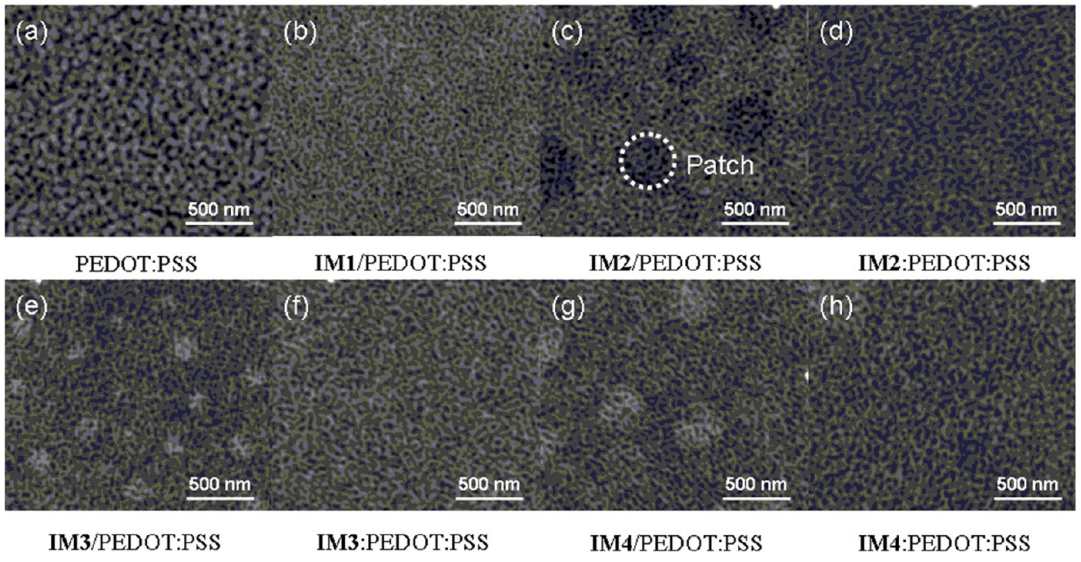

Figure 5. 15 keV HAADF STEM images of FHBC:PCBM blend films on different substrates (a) PEDOT:PSS; (b, c, e, g) **IM**/PEDOT:PSS, and (d, f, h) **IM**:PEDOT:PSS. All films have the same magnification, the scale bar is 500 nm.

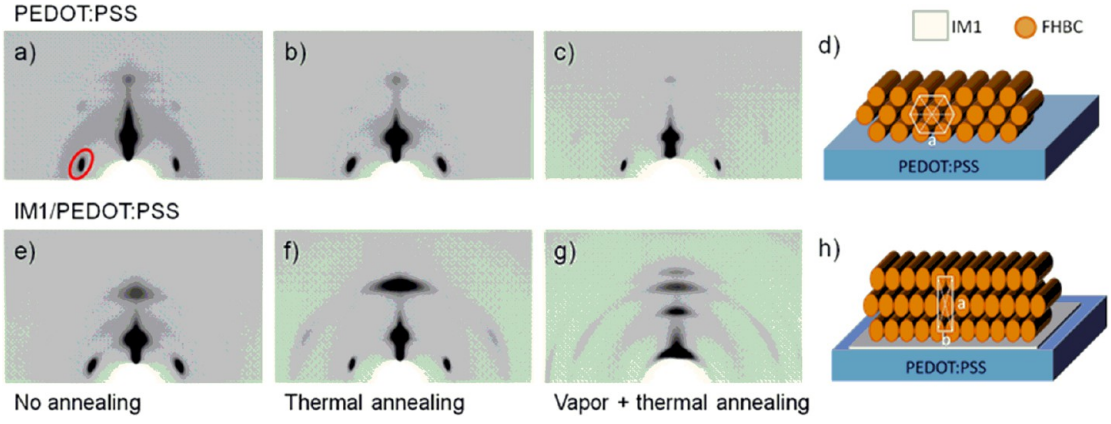

Figure 6. 2D GIWAXS images of FHBC films spin-coated on top of PEDOT:PSS and **IM1**/PEDOT:PSS substrates. (a, e) without annealing (010 reflection is indicated by red circle), (b, f) after thermal annealing at 150 °C for 30 s, and (c, g) after DCB vapor annealing for 24 h followed by thermal annealing at 150 °C for 30 s. Panels d and h are schematic representations of the FHBC molecular packing modes on PEDOT:PSS and **IM1**/PEDOT:PSS films, respectively (the **IM1** interlayer is presented as a gray layer without structural details).

dense than PCBM, hence the FHBC phase appears brighter in the bright-field (BF) TEM images. From Figure 4, it can be observed that FHBC and PCBM can spontaneously phase separate into nanodomains. More importantly, all IMs are able to reduce the domain size in the FHBC:PCBM bulk heterojunction, when comparing Figure 4a with b–h. The IMs could serve as many nucleation sites for the donor molecules resulting in an increase in the number of crystals and, hence, smaller domain sizes. Better understanding will require further future investigations.

Low-energy HAADF STEM is an imaging technique capable of distinguishing organic materials having only a minor difference in average atomic numbers and material densities and can provide an improved contrast between FHBC and PCBM as compared to conventional TEM.[36] PCBM scatters more electrons than FHBC, resulting in a brighter contrast in HAADF STEM images, which is the inverse contrast to that of BF TEM images. Figure 5 confirms the observation, made by TEM, of the reduced domain size after interface modification. A quantitative analysis on the domain sizes can be derived from these images by Fourier transform analysis. Radially averaged two-dimensional discrete Fourier transform analysis of the HAADF STEM images showed quasi-periodic structures that were proportional to the average domain size and domain size within the layer (Supporting Information Figure S3).[4,37] A decrease of the mean phase separation from 51 nm to around 36 nm can be deduced from the peak of the Fourier amplitude of the respective HAADF STEM images and is qualitatively confirmed by the corresponding TEM images. The reduction in domain size helps to create more interface area between FHBC and PCBM, which is beneficial for charge generation in OPV devices.

Interestingly, bright or dark patches are observed in the films containing a spin-coated IM interlayer (Figure 5c, e, and g). The origin of these patches is unclear at the moment and will need further investigation. For the time being, it is important to point out that the contrast in HAADF STEM images is also sensitive to the thickness of the TEM sample.[38] It is possible that the spin-coated IMs can be partially dissolved by chlorobenzene during film formation process of the FHBC:PCBM layer. These IMs can reaggregate and cause variation of the local thickness of the FHBC:PCBM layer,

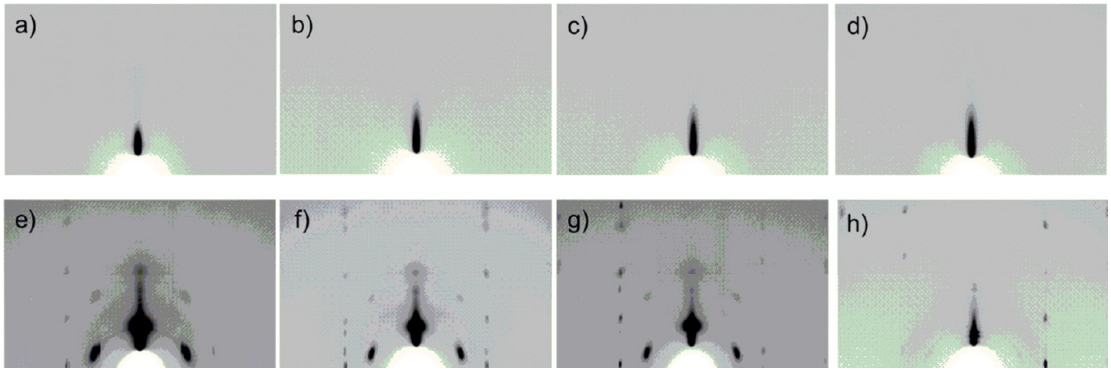

Figure 7. 2D GIWAXS images of modified substrates of (a) **IM3**/PEDOT:PSS, (b) **IM3**:PEDOT:PSS, (c) **IM2**:PEDOT:PSS, (d) **IM4**:PEDOT:PSS, and (e, f, g, and h) FHBC deposited on top of the modified surface followed by vapor and thermal annealing.

inducing local thickness variations resulting in bright and dark patches.

We also employed TEM tomography to construct 3D models of the FHBC:PCBM films on PEDOT:PSS and **IM3**/PEDOT:PSS (Supporting Information Figure S4 and movie). The FHBC donor and PCBM acceptor formed a bicontinuous network on nanoscale throughout the film. Larger domain sizes were observed in the films on non-modified PEDOT:PSS as compared to those on a **IM3**/PEDOT:PSS surface, which is consistent with TEM and HAADF-STEM results.

Thin Film Characterization of FHBC Pure Films. It is anticipated that the IMs will have strong intermolecular interactions with the FHBC donor molecules, as a result of $\pi-\pi$ interactions. Therefore, the influence of the IMs on the molecular order of FHBC pure films were examined using grazing incidence wide-angle X-ray scattering (GIWAXS) (Figure 6). The films were either thermally annealed at 150 °C for 30 s or exposed to a combination of vapor and thermal annealing, while the untreated film serves as a reference. The vapor and thermal annealing was carried out by storing the as-cast FHBC films in a closed Petri dish filled with 1,2-dichlorobenzene (DCB) vapor for 24 h, and then annealing the films at 150 °C for 30 s. It is expected that the vapor of DCB allows the FHBC film to fully relax to a thermodynamic equilibrium state as has been reported for other analogues systems.[39] The thermal annealing step following the vapor annealing serves to remove any residual solvent from the film.

The FHBC layer on PEDOT:PSS exhibits a typical liquid crystalline discotic columnar phase with short-range order as evident from reflections only up to second order (Figure 6a).[40−42] The hexagonal arrangement of the reflections implies a hexagonal packing of FHBC columns with a unit-cell parameter of 2.55 nm of edge-on arranged molecules, whereby the columnar axis is oriented parallel to the surface as illustrated in Figure 6d.[24,43−45] This morphology is not changed after thermal annealing alone or a combination of solvent vapor annealing followed by thermal annealing. Most likely this particular morphology is a thermodynamic minimum when PEDOT:PSS is used as a substrate, since the unit cell parameters remain almost unchanged (Figure 6b,c, decrease of a_{hex} to 2.40 nm for the DCB vapor and thermal annealed film). Furthermore, thermal or vapor and thermal annealing improves crystalline packing of FHBC molecules, as evident from the full width at half-maximum (fwhm) values (Supporting Information Figure S5) in radial (ξ) and azimuthal (ψ) directions extracted from the 010 reflection (indicated in Figure 6a). According to the Scherrer's law, ξ is inversely proportional to the coherence length of molecules in a stack; and ψ is proportional to the angular distribution of diffraction planes in a domain. The reduced ξ and ψ after annealing implies FHBC molecules form more ordered crystalline domains with higher anisotropy.

When an interlayer consisting of **IM1** is present (Figure 6e and f and Supporting Information Figure S5), the size of the hexagonal lattice and the crystallinity persists in comparison to the films without interlayer prepared and treated in the same way. However, after vapor and thermal annealing, the scattering pattern changes significantly and new reflections in the meridional plane appear while most of the hexagonal reflective spots disappear (Figure 6g). These results indicate loss of the original hexagonal packing and the emergence of a new rectangular packing configuration (unit cell parameters a = 6.00 nm and b = 1.90 nm) which has multiple layers that are parallel to the substrate to form a laminar structure as illustrated in Figure 6h. The structural analysis of the peak integration indicates that this new unit cell packing likely coexists with the hexagonal packing (a_{hex}= 2.63 nm), since some of the characteristic features of the hexagonal diffraction pattern are still present. The partial transfer of the liquid crystalline hexagonal to a more crystalline rectangular lattice is accompanied by a slight molecular tilting of the discs of approximately 15−25° toward the columnar axis (Supporting Information Figure S7). Typically for discotics in the bulk solid state at the phase transition between crystalline and liquid crystalline phase, a change in the intracolumnar arrangement from a tilted to a non-tilted packing motif occurs which induces also a lattice modification.[46,47] The additional **IM1** interlayer seems to surface induce partly a crystalline phase following similar phase transition structural changes as in the bulk. Since the X-ray beam penetrates the entire film thickness, it is not possible to differentiate the locations of the two unit cells. The morphologies might consist of two interpenetrated phases, or more probably of a horizontal separation with one phase (probably the rectangular one), preferentially growing at the surface interface.

The organization in FHBC films spin-coated on top of **IM2−4**/PEDOT:PSS and **IM2−4**:PEDOT:PSS substrates were examined with GIWAXS as well. All the films were treated with vapor and thermal annealing to achieve the quasi-equilibrium state. As can be seen from Figures 7a-d the small amount of IMs present on PEDOT:PSS does not contribute to any X-ray diffraction patterns. Therefore, no structural details for the interlayers can be derived from this data. The presence of an interlayer does, however, result in new distinct features in

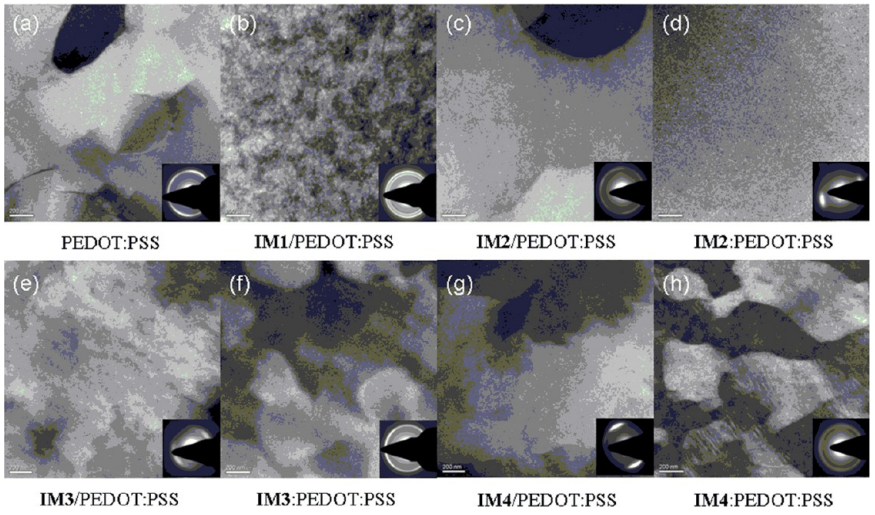

Figure 8. 300 keV dark-field TEM images of vapor + thermally annealed FHBC films on various substrates (a) PEDOT:PSS; (b, c, e, g) **IM**/PEDOT:PSS and (d, f, h) **IM**:PEDOT:PSS. The scale bar is 200 nm, the inset is the SAED pattern of the corresponding sample.

the patterns. Unlike the patterns produced by **IM1**/PEDOT:PSS (Figure 6g), interface modification by **IM2**, **IM3**, or **IM4** induces a morphological change in the FHBC layer resulting in a number of vertical Bragg rods that extend in the q_z direction (Figure 7e–h).

These Bragg rods imply again the coexistence of two phases in the thin film. Interestingly, the Bragg rods in the GIWAXS images of the films which contain an IM interlayer (Figure 7e and Supporting Information Figures S8 and S9) that has been spin-coated onto the PEDOT:PSS, are significantly less prominent in comparison to the images of films that have an interlayer originating from an IM:PEDOT:PSS blend (Figures 7f–h). From the GIWAXS pattern, the hexagonal liquid crystalline unit cell is derived with a parameter a_{hex} of 2.56 nm. The second, more crystalline phase gives distinct Bragg rods with large number of high order reflections which are arranged parallel to the meridional axis. In this phase, the FHBC columns are oriented parallel to the surface with also edge-on arrangement. However, the obtained data does not allow us to determine a precise unit cell, neither the exact location within the film. However, it can be assumed that the crystallization might occur preferentially at the interface between IM and FHBC. Thereby, the flexible PEG substituents of **IM2**–**4** might play an important role by favoring the crystallization of the FHBC molecules into large ordered domains on the surface. It is known that additional dielectric surface treatment of transistors with self-assembled monolayers (SAMs) also improves the nucleation and growth of organic semiconductors.[48,49]

The crystalline grains in the FHBC films were further studied with TEM. The dark-field TEM images in Figure 8 are sensitive to the crystalline orientation of the grains. After vapor and thermal annealing, the FHBC film on PEDOT:PSS substrate contains grains with an average size of more than 300 nm (Figure 8a). The grain boundaries are sharp and clear. The diffraction ring in selected area electron diffraction (SAED) corresponds to a *d*-spacing of 0.35 nm, which matches with the intermolecular stacking distance in a FHBC crystal.[19] It can be seen that the **IM1** interlayer reduces the grain size of the FHBC layer and leads to less well-defined grain boundaries. Interestingly, in its SAED pattern an additional smaller diffraction ring is present which corresponds to a *d*-spacing of 0.39 nm. This *d*-spacing matches with the *d*-spacing of 0.40 nm observed in GIWAXS diffractogram (Supporting Information Figure S7) and can be ascribed to the π–π distance in the FHBC rectangular packing. To identify the new molecular configuration, a TEM image was taken at higher magnification for this sample (Supporting Information Figure S10). Two different structures can be identified, i.e. parallel fringes and web-like nanofibers. The parallel fringes are due to crystalline FHBC columns, which have been observed previously.[50] The web-like nanofibers, however, have not been seen before and are only present in the FHBC/**IM1**/PEDOT:PSS thin film stack. It is possible that the nanofibers are the result of the rectangular packing structure of FHBC in a similar manner as has been reported for the semicrystalline poly(3-hexylthiophene) (P3HT).[51]

The presence of a spin-coated interlayer of IM, that is, in the FHBC/IM/PEDOT:PSS films, results in an increase in grain size (see also SAED patterns) of FHBC as compared to the FHBC/PEDOT:PSS film (insets of Figure 8c, e, and g). The intensity of the diffraction ring of the inserted SAED pattern in Figure 8a is almost constant in all directions, whereas it becomes stronger in certain directions for the FHBC/**IM3**/PEDOT:PSS and FHBC/**IM4**/PEDOT:PSS films (Figure 8c, e, and g). The TEM analysis also showed a significant change in the crystalline nature between FHBC films deposited onto pristine PEDOT:PSS and **IM2**:PEDOT:PSS. The presence of the **IM2** interlayer results in a FHBC film with a close to homogeneous crystalline orientation as indicated by the localized intensity of the diffraction ring obtained from the latter film.

Single-Crystal Characterization of FHBC. To better understand the crystallization of FHBC materials in thin films, single crystals of FHBC were grown by slow evaporation of isopropanol into a dichloromethane solution (Figure 9 and Supporting Information). The asymmetric unit consists of one unique molecule of FHBC which is π-stacked above and below to two half molecules of FHBC which sit on crystallographic inversion centers, the three π-systems are close to parallel. The interplanar spacings are ~3.42 and 3.04 Å and the corresponding centroid to centroid distances between the central hexabenzocoronene ring and the two flanking molecules are 4.141 and 4.498 Å, respectively, indicating a certain amount

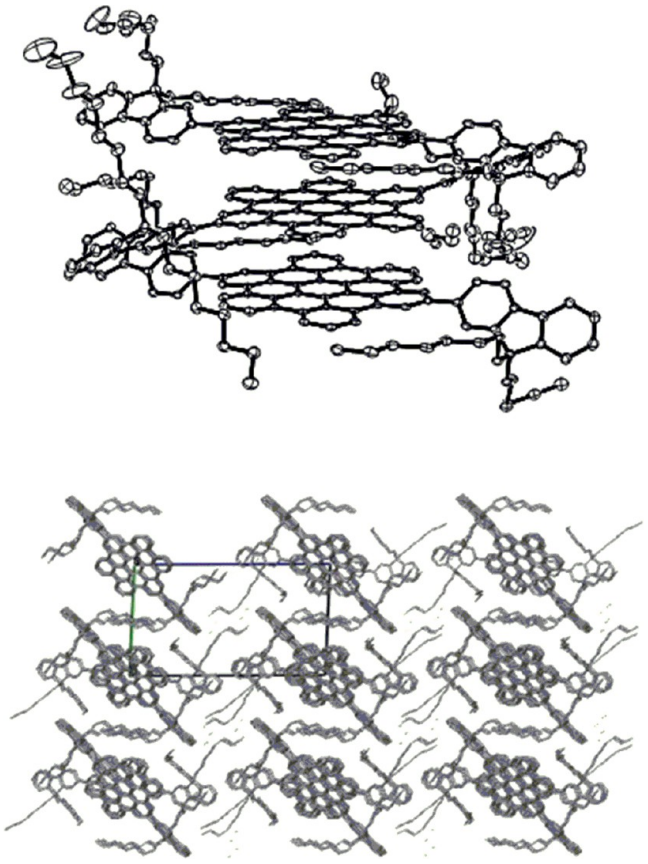

Figure 9. Thermal ellipsoid plot of the structure of FHBC (top) and crystal packing diagram (bottom) extending down the *a*-axis. Triclinic, space group $P\bar{1}$, a = 17.2331(8) Å, b = 17.2446(7) Å, c =27.9818(14) Å, α = 92.121(4)°, β = 91.996(4)°, γ = 112.639(4)°.

of slippage of the π-stacked ring systems. The structure contains three molecules of dichloromethane, which is disordered.

The length data extracted from the single crystal analysis, however (except for the $\pi-\pi$ stacking distance) do not correspond any of the length data for the thin films extracted from the GIWAXS analysis indicating significantly different crystalline forms and that factors governing the crystallization process in thin films of FHBC appear to be significantly different to those in solution.

CONCLUSION

We demonstrate that blending a small amount (0.2 wt %) of amphiphilic interface modifier (IM) into PEDOT:PSS can have a profound effect on the morphology of the layer that is deposited on top of it. A blended IM is able to change the crystal packing of a pure film of donor materials, that is, FHBC, or it can reduce the domain sizes in the active layer consisting of FHBC and PCBM respectively. This is, likely, the result of the assembly of the IMs onto the surface of the PEDOT:PSS via diffusion and its, subsequent, templating effect on the active layer (i.e., donor or donor:acceptor blend). For OPV devices having an active layer consisting of FHBC:PCBM, the insertion of an IM templating layer can lead to over 20% enhancement in photovoltaic performance. We believe that the spontaneous surface diffusion and assembly of amphiphilic compounds that have been blended into PEDOT:PSS could be a powerful strategy to advantageously change characteristics of the active layer such as morphology.

ASSOCIATED CONTENT

Supporting Information

Experimental section including synthesis, CV spectra, GIWAXS graphs, TEM bright field image, and FHBC single crystal X-ray data. This material is available free of charge via the Internet at http://pubs.acs.org

AUTHOR INFORMATION

Corresponding Authors

*E-mail: wwhwong@unimelb.edu.au.
*E-mail: djjones@unimelb.edu.au.

Author Contributions

H.H.D. and K.S. contributed equally to this work. All authors have given approval to the final version of the manuscript.

Notes

The authors declare no competing financial interest.

ACKNOWLEDGMENTS

The authors are grateful to Scott Watkins and Thomas Gengenbach from the Commonwealth Science and Industrial Research Organisation (CSIRO) for their help on the PESA measurements and contribution in the form of discussions. The authors are also grateful to the Australian Renewable Energy Agency (ARENA) for financial support and to the Australian Synchrotron for providing the GIWAXS beamtime.

REFERENCES

(1) Scully, S. R.; McGehee, M. D. Effects of Optical Interference and Energy Transfer on Exciton Diffusion Length Measurements in Organic Semiconductors. *J. Appl. Phys.* **2006**, *100*, 034907−1−034907−5.

(2) Lunt, R. R.; Giebink, N. C.; Belak, A. A.; Benziger, J. B.; Forrest, S. R. Exciton Diffusion Lengths of Organic Semiconductor Thin Films Measured by Spectrally Resolved Photoluminescence Quenching. *J. Appl. Phys.* **2009**, *105*, 053711−1−053711−7.

(3) Savenije, T. J.; Kroeze, J. E.; Yang, X.; Loos, J. The Effect of Thermal Treatment on the Morphology and Charge Carrier Dynamics in a Polythiophene−Fullerene Bulk Heterojunction. *Adv. Funct. Mater.* **2005**, *15*, 1260−1266.

(4) Liu, R.; Wu, D.; Feng, X.; Müllen, K. Bottom-Up Fabrication of Photoluminescent Graphene Quantum Dots with Uniform Morphology. *J. Am. Chem. Soc.* **2011**, *133*, 15221−15223.

(5) Li, G.; Yao, Y.; Yang, H.; Shrotriya, V.; Yang, G.; Yang, Y. Solvent Annealing Effect in Polymer Solar Cells Based on Poly(3-hexylthiophene) and Methanofullerenes. *Adv. Funct. Mater.* **2007**, *17*, 1636−1644.

(6) Miller, S.; Fanchini, G.; Lin, Y.-Y.; Li, C.; Chen, C.-W.; Su, W.-F.; Chhowalla, M. Investigation of Nanoscale Morphological Changes in Organic Photovoltaics During Solvent Vapor Annealing. *J. Mater. Chem.* **2008**, *18*, 306−312.

(7) Fang, G.; Liu, J.; Fu, Y.; Meng, B.; Zhang, B.; Xie, Z.; Wang, L. Improving the Nanoscale Mophology and Pocessibility for PCDTBT-based Polymer Solar Cells via Solvent Mixtures. *Org. Electron.* **2012**, *13*, 2733−2740.

(8) Chu, T.-Y.; Alem, S.; Tsang, S.-W.; Tse, S.-C.; Wakim, S.; Lu, J.; Dennler, G.; Waller, D.; Gaudiana, R.; Tao, Y. Morphology Control in Polycarbazole based Bulk Heterojunction Solar Cells and its Impact on Device Performance. *Appl. Phys. Lett.* **2011**, *98*, 253301−1−253301−3.

(9) Ouyang, J.; Xia, Y. High-Performance Polymer Photovoltaic Cells with Thick P3HT:PCBM Films Prepared by a Quick Drying Process. *Sol. Energy Mater. Sol. Cells* **2009**, *93*, 1592−1597.

(10) Ye, L.; Zhang, S.; Ma, W.; Fan, B.; Guo, X.; Huang, Y.; Ade, H.; Hou, J. From Binary to Ternary Solvent: Morphology Fine-tuning of D/A Blends in PDPP3T-Based Polymer Solar Cells. *Adv. Mater.* **2012**, *24*, 6335−6341.
(11) Peet, J.; Kim, J. Y.; Coates, N. E.; Ma, W. L.; Moses, D.; Heeger, A. J.; Bazan, G. C. Efficiency Enhancement in Low-Bandgap Polymer Solar Cells by Processing with Alkane Dithiols. *Nat. Mater.* **2007**, *6*, 497−500.
(12) Liu, X.; Huettner, S.; Rong, Z.; Sommer, M.; Friend, R. H. Solvent Additive Control of Morphology and Crystallization in Semiconducting Polymer Blends. *Adv. Mater.* **2012**, *24*, 669−674.
(13) Guo, X.; Cui, C.; Zhang, M.; Huo, L.; Huang, Y.; Hou, J.; Li, Y. High Efficiency Polymer Solar Cells based on Poly(3-hexylthiophene)/Indene-C70 bisadduct with Solvent Additive. *Energy Environ. Sci.* **2012**, *5*, 7943−7949.
(14) Graham, K. R.; Stalder, R.; Wieruszewski, P. M.; Patel, D. G.; Salazar, D. H.; Reynolds, J. R. Tailor-Made Additives for Morphology Control in Molecular Bulk-Heterojunction Photovoltaics. *ACS Appl. Mater. Interfaces* **2013**, *5*, 63−71.
(15) Warman, J. M.; Van De Craats, A. M. Charge Mobility in Discotic Materials Studied by Pr-Trmc. *Mol. Cryst. Liq. Cryst.* **2003**, *396*, 41−72.
(16) Piris, J.; Debije, M. G.; Stutzmann, N.; Laursen, B. W.; Pisula, W.; Watson, M. D.; BjØrnholm, T.; Müllen, K.; Warman, J. M. Aligned Thin Films of Discotic Hexabenzocoronenes: Anisotropy in the Optical and Charge Transport Properties. *Adv. Funct. Mater.* **2004**, *14*, 1053−1061.
(17) Feng, X.; Marcon, V.; Pisula, W.; Hansen, M. R.; Kirkpatrick, J.; Grozema, F.; Andrienko, D.; Kremer, K.; Müllen, K. Towards High Charge-Carrier Mobilities by Rational Design of the Shape and Periphery of Discotics. *Nat. Mater.* **2009**, *8*, 421−426.
(18) Pisula, W.; Feng, X.; Müllen, K. Charge-Carrier Transporting Graphene-Type Molecules. *Chem. Mater.* **2011**, *23*, 554−567.
(19) Pisula, W.; Zorn, M.; Chang, J. Y.; Müllen, K.; Zentel, R. Liquid Crystalline Ordering and Charge Transport in Semiconducting Materials. *Macromol. Rapid Commun.* **2009**, *30*, 1179−1202.
(20) Liu, C. Y.; Fechtenkötter, A.; Watson, M. D.; Müllen, K.; Bard, A. J. Room Temperature Discotic Liquid Crystalline Thin Films of Hexa-peri-hexabenzocoronene: Synthesis and Optoelectronic Properties. *Chem. Mater.* **2003**, *15*, 124−129.
(21) Seyler, H.; Purushothaman, B.; Jones, D. J.; Holmes, A. B.; Wong, W. W. H. Hexa-*peri*-hexabenzocoronene in Organic Electronics. *Pure Appl. Chem.* **2012**, *84*, 1047−1067.
(22) Kastler, M.; Pisula, W.; Wasserfallen, D.; Pakula, T.; Müllen, K. Influence of the Alkyl Substituents on the Solution and Surface-Organization of Hexabenzocoronenes. *J. Am. Chem. Soc.* **2005**, *127*, 4286−4295.
(23) Pisula, W.; Kastler, M.; Wasserfallen, D.; Mondeshki, M.; Piris, J.; Schnell, I.; Müllen, K. Relation between Supramolecular Order and Charge Carrier Mobility of Branched Alkyl Hexa-*peri*-hexabenzocoronenes. *Chem. Mater.* **2006**, *18*, 3634−3640.
(24) Wong, W. W. H.; Singh, T. B.; Vak, D.; Pisula, W.; Yan, C.; Feng, X.; Williams, E. L.; Chan, K. L.; Mao, Q.; Jones, D. J.; Ma, C.-Q.; Müllen, K.; Bäuerle, P.; Holmes, A. B. Solution Processable Fluorenyl Hexa-*peri*-hexabenzocoronenes in Organic Field-Effect Transistors and Solar Cells. *Adv. Funct. Mater.* **2010**, *20*, 927−938.
(25) Pisula, W.; Tomovic, Z.; El Hamaoui, B.; Watson, M. D.; Pakula, T.; Müllen, K. Control of the Homeotropic Order of Hexa-*peri*-benzocoronenes. *Adv. Funct. Mater.* **2005**, *15*, 893−904.
(26) Friedlein, R.; Crispin, X.; Simpson, C.; Watson, M.; Jäckel, F.; Osikowicz, W.; Marciniak, S.; de Jong, M.; Samorí, P.; Jönsson, S.; Fahlman, M.; Müllen, K.; Rabe, J.; Salaneck, W. Electronic Structure of Highly Ordered Films of Self-Assembled Graphitic Nanocolumns. *Phys. Rev. B* **2003**, *68*, 195414−195417.
(27) Samorý, P.; Keil, M.; Friedlein, R.; Birgerson, J.; Brand, J. D.; Müllen, K.; Salaneck, W. R.; Rabe, J. P. Growth of Ordered Hexakis-dodecyl-hexabenzocoronene Layers from Solution: A SFM and ARUPS Study. *J. Phys. Chem. B* **2001**, 11114−11119.
(28) Ruffieux, P.; Gröning, O.; Bielmann, M.; Simpson, C.; Müllen, K.; Schlapbach, L.; Gröning, P. Supramolecular Columns of Hexabenzocoronenes on Copper and Gold (111) Surfaces. *Phys. Rev. B* **2002**, *66*, 073409−073404.
(29) Kremer, J. R.; Mastronarde, D. N.; McIntosh, J. R. Computer Visualization of Three-Dimensional Image Data Using IMOD. *J. Struct. Biol.* **1996**, *116*, 71−76.
(30) http://bio3d.colorado.edu/.
(31) Hughes, J. M.; Hernandez, Y.; Aherne, D.; Doessel, L.; Müllen, K.; Moreton, B.; White, T. W.; Partridge, C.; Costantini, G.; Shmeliov, A.; Shannon, M.; Nicolosi, V.; Coleman, J. N. High Quality Dispersions of Hexabenzocoronene in Organic Solvents. *J. Am. Chem. Soc.* **2012**, *134*, 12168−12179.
(32) Xia, Y. J.; Ouyang, J. Y. PEDOT:PSS Films with Significantly Enhanced Conductivities Induced by Preferential Solvation with Cosolvents and their Application in Polymer Photovoltaic Cells. *J. Mater. Chem.* **2011**, *21*, 4927−4936.
(33) Ouyang, J.; Xu, Q.; Chu, C.-W.; Yang, Y.; Li, G.; Shinar, J. On the Mechanism of Conductivity Enhancement in Poly(3,4-ethylenedioxythiophene):poly(styrene sulfonate) Film through Solvent Treatment. *Polymer* **2004**, *45*, 8443−8450.
(34) Wang, T.; Qi, Y.; Xu, J.; Hu, X.; Chen, P. Effects of Poly(ethylene glycol) on Electrical Conductivity of Poly(3,4-ethylenedioxythiophene)−Poly(styrenesulfonic acid) Film. *Appl. Surf. Sci.* **2005**, *250*, 188−194.
(35) Zhou, Y. H.; Li, F. H.; Barrau, S.; Tian, W. J.; Inganas, O.; Zhang, F. L. Inverted and Transparent Polymer Solar Cells Prepared with Vacuum-Free Processing. *Sol. Energy Mater. Sol. Cells* **2009**, *93*, 497−500.
(36) Pfaff, M.; Klein, M. F.; Muller, E.; Muller, P.; Colsmann, A.; Lemmer, U.; Gerthsen, D. Nanomorphology of P3HT:PCBM-based Absorber Layers of Organic Solar Cells after Different Processing Conditions Analyzed by Low-Energy Scanning Transmission Electron Microscopy. *Microsc. Microanal.* **2012**, *18*, 1380−1388.
(37) Ma, W.; Yang, C.; Heeger, A. J. Spatial Fourier-Transform Analysis of the Morphology of Bulk Heterojunction Materials Used in "Plastic" Solar Cells. *Adv. Mater.* **2007**, *19*, 1387−1390.
(38) Pfaff, M.; Muller, E.; Klein, M. F.; Colsmann, A.; Lemmer, U.; Krzyzanek, V.; Reichelt, R.; Gerthsen, D. Low-Energy Electron Scattering in Carbon-Based Materials Analyzed by Scanning Transmission Electron Microscopy and its Application to Sample Thickness Determination. *J. Microsc.* **2011**, *243*, 31−39.
(39) Li, G.; Shrotriya, V.; Huang, J.; Yao, Y.; Moriarty, T.; Emery, K.; Yang, Y. High-Efficiency Solution Processable Polymer Photovoltaic Cells by Self-Organization of Polymer Blends. *Nat. Mater.* **2005**, *4*, 864−868.
(40) Kouwer, P. H. J.; van den Berg, O.; Jager, W. F.; Mijs, W. J.; Picken, S. J. Induced Liquid Crystalline Diversity in Molecular and Polymeric Charge-Transfer Complexes of Discotic Mesogens. *Macromolecules* **2002**, *35*, 2576−2582.
(41) Jeong, K.-U.; Jing, A. J.; Monsdorf, B.; Graham, M. J.; Harris, F. W.; Cheng, S. Z. D. Self-Assembly of Chemically Linked Rod−Disc Mesogenic Liquid Crystals. *J. Phys. Chem. B* **2007**, *111*, 767−777.
(42) Shu, J.; Dudenko, D.; Esmaeili, M.; Park, J. H.; Puniredd, S. R.; Chang, J. Y.; Breiby, D. W.; Pisula, W.; Hansen, M. R. Coexistence of Helical Morphologies in Columnar Stacks of Star-Shaped Discotic Hydrazones. *J. Am. Chem. Soc.* **2013**, *135*, 11075−11086.
(43) Tracz, A.; Jeszka, J. K.; Watson, M. D.; Pisula, W.; Müllen, K.; Pakula, T. Uniaxial Alignment of the Columnar Super-Structure of a Hexa (Alkyl) Hexa-*peri*-hexabenzocoronene on Untreated Glass by Simple Solution Processing. *J. Am. Chem. Soc.* **2003**, *125*, 1682−1683.
(44) Pouzet, E.; Cupere, V. D.; Heintz, C.; Andreasen, J. W.; Breiby, D. W.; Nielsen, M. M.; Viville, P.; Lazzaroni, R.; Gbabode, G.; Geerts, Y. H. Homeotropic Alignment of a Discotic Liquid Crystal Induced by a Sacrificial Layer. *J. Phys. Chem. C* **2009**, *113*, 14398−14406.
(45) Bunk, O.; Nielsen, M. M.; Solling, T. I.; van de Craats, A. M.; Stutzmann, N. Induced Alignment of a Solution-Cast Discotic Hexabenzocoronene Derivative for Electronic Devices Investigated by Surface X-ray Diffraction. *J. Am. Chem. Soc.* **2003**, *125*, 2252−2258.

(46) Sergeyev, S.; Pisula, W.; Geerts, Y. H. Discotic Liquid Crystals: A New Generation of Organic Semiconductors. *Chem. Soc. Rev.* **2007**, *36*, 1902−1929.
(47) Laschat, S.; Baro, A.; Steinke, N.; Giesselmann, F.; Hägele, C.; Scalia, G.; Judele, R.; Kapatsina, E.; Sauer, S.; Schreivogel, A.; Tosoni, M. Discotic Liquid Crystals: From Tailor-Made Synthesis to Plastic Electronics. *Angew. Chem., Int. Ed.* **2007**, *46*, 4832−4887.
(48) Yang, H.; Shin, T. J.; Ling, M.-M.; Cho, K.; Ryu, C. Y.; Bao, Z. Conducting AFM and 2D GIXD Studies on Pentacene Thin Films. *J. Am. Chem. Soc.* **2005**, *127*, 11542−11543.
(49) DiBenedetto, S. A.; Facchetti, A.; Ratner, M. A.; Marks, T. J. Molecular Self-Assembled Monolayers and Multilayers for Organic and Unconventional Inorganic Thin-Film Transistor Applications. *Adv. Mater.* **2009**, *21*, 1407−1433.
(50) Pfaff, M.; Müller, P.; Bockstaller, P.; Müller, E.; Subbiah, J.; Wong, W. W. H.; Klein, M. F. G.; Kiersnowski, A.; Puniredd, S. R.; Pisula, W.; Colsmann, A.; Gerthsen, D.; Jones, D. J. Bulk Heterojunction Nanomorphology of Fluorenyl Hexa-*peri*-hexabenzocoronene−Fullerene Blend Films. *ACS Appl. Mater. Interfaces* **2013**, *5*, 11554−11562.
(51) Brinkmann, M.; Wittmann, J. C. Orientation of Regioregular Poly(3-hexylthiophene) by Directional Solidification: A Simple Method to Reveal the Semicrystalline Structure of a Conjugated Polymer. *Adv. Mater.* **2006**, *18*, 860−863.